In vivo thickness and birefringence determination of the human retinal nerve fiber layer using polarization-sensitive optical coherence tomography

CENSE B.[1], CHEN T.C.[2], DE BOER J.F.[1]

ABSTRACT

Thinning of the retinal nerve fiber layer and changes in retinal nerve fiber layer birefringence may both precede clinically detectable glaucomatous vision loss. We present in vivo thickness and depth-resolved birefringence measurements of the human retinal nerve fiber layer (RNFL) by use of polarization-sensitive optical coherence tomography (PS-OCT). Using a fiber-based PS-OCT setup real-time images of the human retina in vivo were recorded, co-registered with retinal video images of the location of PS-OCT scans. PS-OCT scans around the optic nerve head (ONH) of two healthy young volunteers were made using 10 concentric circles of increasing radius. Both the mean retinal nerve fiber layer thickness and mean retinal nerve fiber birefringence for each of 48 sectors on a circle were determined. The retinal nerve fiber layer thickness and birefringence varied as a function of sector around the ONH. Measured double pass phase retardation per unit depth values around the ONH range between 0.10 and 0.35°/μm. The retinal nerve fiber layer becomes thinner with increasing distance from the ONH. In contrast, the birefringence does not vary significantly with increasing distance from the ONH.

KEY WORDS

Birefringence, glaucoma, retinal nerve fiber layer, polarization sensitive optical coherence tomography

RÉSUMÉ

L'amincissement de la couche de fibres nerveuses rétiniennes et les changements de biréfringence de la couche de fibres nerveuses rétiniennes peuvent tous deux être les signes avant-coureurs d'une perte de vision glaucomateuse détectable cliniquement. Nous présentons des mesures in vivo de l'épaisseur et de la biréfringence à résolutions en profondeur de la couche de fibres nerveuses rétiniennes (CNFR) chez l'humain par utilisation de la tomographie par cohérence optique sensible à la polarisation (TCO-SP). En utilisant un réglage TCO-SP sur fibres, des images en temps réel de la rétine humaine in vivo ont été enregistrées, co-enregistrées avec des images vidéo rétiniennes de l'emplacement des balayages TCO-SP. Des balayages TCO-PS autour de la tête du nerf optique (TNO) de deux jeunes volontaires en bonne santé ont été effectués en utilisant 10 cercles concentriques de rayon croissant. Aussi bien l'épaisseur moyenne de la couche de fibres nerveuses rétiniennes que la biréfringence moyenne de la couche de fibres nerveuses rétiniennes pour chacun des 48 secteurs d'un cercle ont été déterminées. L'épaisseur et la biréfringence de la couche de fibres nerveuses rétiniennes varient en fonction du secteur autour de la TNO. Le retard de phase double passage mesuré par valeurs unitaires de profondeur autour de la TNO varie entre 0,10 et 0,35°/μm. La

.....

[1] *Harvard Medical School and Wellman Center for Photomedicine, MGH, Boston, MA*
[2] *Massachusetts Eye and Ear Infirmary and Harvard Medical School, Boston, MA*

couche de fibres nerveuses rétiniennes s'amincit à mesure que la distance depuis la TNO s'accroît. En revanche, la biréfringence ne varie pas significativement en fonction du rayon.

MOTS-CLÉS

Biréfringence, glaucome, couche de fibres nerveuses rétiniennes, tomographie par cohérence optique sensible à la polarisation

INTRODUCTION

Glaucoma is the world's second leading cause of blindness. The disease causes damage to the retinal ganglion cells, resulting in thinning of the retinal nerve fiber layer (RNFL). In addition, nerve fiber layer tissue loss may be preceded by birefringence changes. As ganglion cells become necrotic and axons in the RNFL are replaced by a less organized and amorphous tissue composed of glial cells,[17] birefringence changes should be expected to occur. When glaucoma is first detected, further loss of vision can often be prevented by treatment. The visual field test is the current standard method of detecting loss of peripheral vision from glaucoma. However, measurements show that up to 40 % of the nerves are irreversibly damaged before loss of peripheral vision can be clinically detected.[17]

There is therefore a need for objective instruments that can detect glaucomatous nerve fiber layer thinning prior to clinically detectable vision loss. Two such instruments that are in development are optical coherence tomography (OCT) and scanning laser polarimetry (SLP). With OCT, cross-sectional structural images of the retina can be made in vivo, allowing determination of the RNFL thickness.[11,19] Variations in optical scattering and absorption allow differentiation between the different layers of the retina. A limitation in RNFL thickness determination by commercial OCT instruments is the axial resolution of about 10 μm.[19] Experimental lab based high-resolution optical coherence tomography (HR-OCT) instruments use a light source with a particularly large optical bandwidth, allowing for RNFL thickness measurements with an accuracy of up to 3 μm.[11] However, current ultra-broadband sources are expensive and complex, and since the signal to noise ratio of an OCT system is inversely proportional to the detection bandwidth and thus the source bandwidth, a reduction in acquisition speed is required, making HR-OCT less appealing for routine examination. Recent development of Spectral Domain/Fourier Domain OCT technology has allowed significant simultaneous increase in speed and resolution, allowing video rate imaging at ultra-high resolution, addressing the speed and resolution limitation of current OCT instruments.[6,15]

In scanning laser polarimetry (SLP), the retina in and around the ONH is probed with polarized light in order to detect RNFL phase retardation and to then indirectly determine RNFL thickness.[22-23] The RNFL is slightly birefringent due to its ordered structure,[24] but birefringence is absent in layers that are located below the RNFL, including the ganglion cell layer. Birefringent elements in the eye such as the cornea and the RNFL change the polarization state of the incident light. The polarization state of light that is reflected back from all retinal structures and that has double-passed the RNFL is compared with the input polarization state. Assuming that RNFL birefringence is constant as a function of location and is constant between subjects, one can calculate RNFL thickness from the measured change in the polarization state or phase retardation of the reflected light.

Polarization-sensitive optical coherence tomography (PS-OCT) combines the depth resolution of OCT with the polarization sensitivity of SLP to image the depth resolved optical birefringence of biological tissue.[7-8,16,18] Glaucomatous loss of nerve fiber tissue may be preceded by a change in birefringence since it is suspected that disintegration of the nerve fiber mesh will lead to a change of RNFL birefringence. Such a change in birefringence compared to normal values could be an early and more specific sign of glaucomatous atrophy of the RNFL.

Ex vivo measurements of primate and enucleated rabbit eyes demonstrated birefringence in the retinal nerve fiber layer and showed good correlation between the thickness determined with PS-OCT and histology.[9-10] Huang and Knighton measured the single-pass phase retardation of isolated rat RNFL.[13] In addition, PSOCT may enhance specificity in determining RNFL thickness in structural OCT images by using changes in tissue birefringence to determine the border between the RNFL and ganglion cell layer. A complicating factor in measuring retinal birefringence is the presence of corneal birefringence, which changes the incident polarization state on the retina unpredictably.[12] In the PS-OCT phase retardation calculation, the surface of the retina is used as a reference, which eliminates corneal contributions.[3-4] In SLP measurements the cor-

neal contribution to the birefringence of the retina is compensated for by use of a variable cornea compensator (VCC).[25]

Phase retardation is related to birefringence and RFNL thickness according to the following equation: *phase retardation = RNFL birefringence × RNFL thickness*. In PS-OCT and SLP the light that scatters back double passes the RNFL before it is detected, which changes the above equation to: *double-pass phase retardation (DPPR) = RNFL birefringence × 2 × RNFL thickness*. The first in vitro RNFL birefringence measurements were reported by Weinreb et al.[22] With SLP they measured two fixed primate eyes with the anterior segments removed and correlated the measured phase retardation with RNFL thickness histology measurements. They found a typical DPPR/UD value of 0.27°/μm. Previously, in vivo PS-OCT measurements were performed on the retina of one healthy subject.[3-4] RNFL thickness and depth-resolved birefringence measurements that were obtained in four blocks around the optic nerve head (ONH) demonstrated that the birefringence or double-pass phase retardation per unit depth (DPPR/UD) is not constant, but varies between 0.18 and 0.37°/μm (J.F. de Boer, IOVS, 2003, 44, ARVO e-abstract, 239). Huang et al. determined RNFL birefringence using an indirect method combining SLP phase retardation measurements and OCT thickness measurements obtained from healthy volunteers in vivo. Assuming that the measuring beam double passes the RNFL, they found a mean DPPR/UD value of 0.37 ± 0.02°/μm. (X. Huang, IOVS, 2003, 44, ARVO e-abstract, 235).

Here we present a summary of in vivo human depth-resolved measurements of RNFL birefringence using PS-OCT.[3-5]

MATERIALS AND METHODS

In order to measure the RNFL birefringence in human subjects in vivo, we used a fiber-based PS-OCT setup that produces real-time images of the retina.[3-4] Fiber-based PS-OCT systems offer the advantage of an easier to construct human eye measurement interface. However, in a fiber-based PS-OCT system, it is difficult to maintain a constant polarization state at the sample surface, since stress in the fibers and a non-circular shape of the fiber core will change the polarization state of the light traveling through the fiber. This problem was overcome by a relative measurement method in which the tissue was probed with two different polarization states, 90° apart on the Poincaré sphere, and generated by means of a piezo-driven polarization modulator in the source arm. A high power super luminescent diode (Superlum Russia) generated a broadband spectrum with a power of 4.6 mW (after polarization) and with a full width half maximum (FWHM) bandwidth of 50 nm centered at 839 nm. The coherence function was measured on a mirror in water (n = 1.33), giving a FWHM coherence length of 5.9 μm. As shown in figure 1, a fiber coupler divided the light between sample and reference arms. The beam splitter ratio in the interferometer was chosen as 70/30, since the power that can be sent into the eye has to be below the ANSI standard limit of 610 μW.[1] The sample arm consisted of a telecentric XY retina scanner and a headrest from a standard slit lamp, with the sample beam pivoting about the center of the entrance pupil of the eye (Fig. 2). Because aberrations are incurred in the cornea and lens, optimal spot size (and therefore maximum retinal reflection) is obtained when the beam has a width of about 2 to 3 mm at the pupil plane.[2] A dichroic beam splitter was used to reflect the sample beam towards a D40 ophthalmic Volk lens positioned 25 mm in front of the cornea. Incident power on the eye was 500 ± 5 μW, well below the maximum level specified in the ANSI standards. The retina was illuminated with an incandescent source of a slit lamp through the dichroic beam splitter. Both PS-OCT beam and illumination beam traveled off-axis through the Volk lens to avoid the strong surface reflections from this lens and the cornea. A charged coupled device (CCD) camera was available for visual inspection of the retina and localization of PS-OCT scans in the retina. During a PS-OCT B-scan, which took 2 seconds, eight CCD images were acquired subsequently and stored to hard disk. While thirty percent of the power was sent to the sample, the remaining seventy percent of the power was directed towards the reference

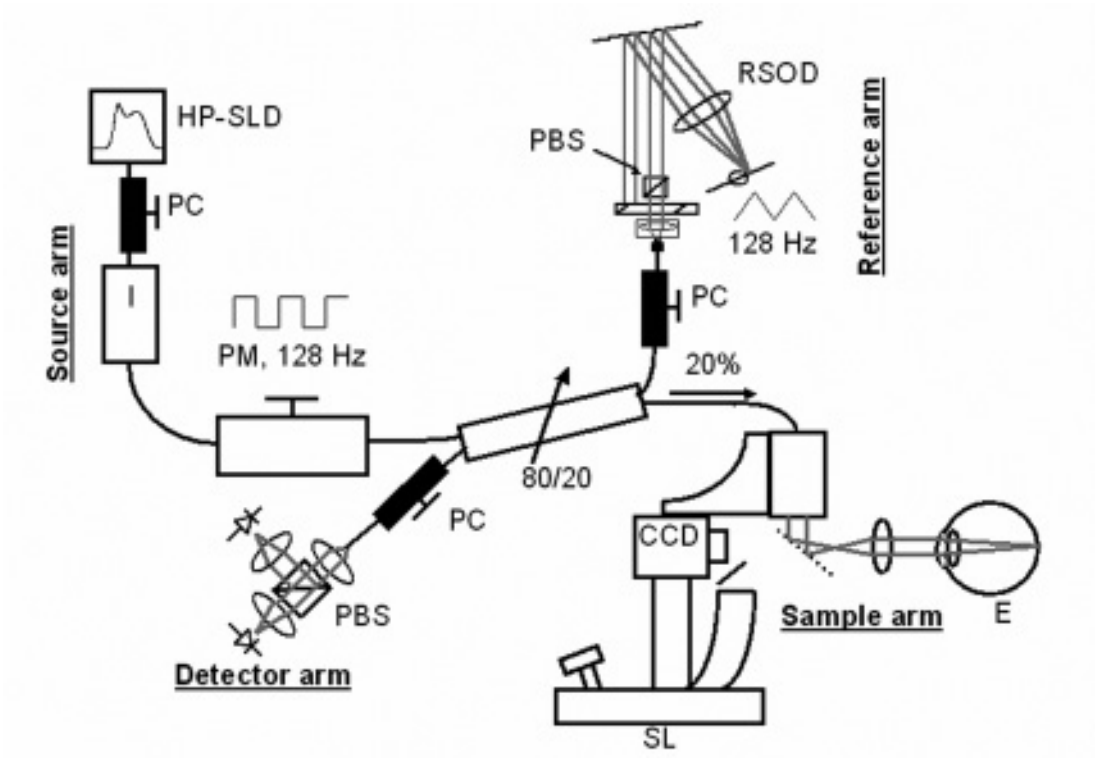

Fig. 1. Schematic of the experimental setup. Light emitted by the super luminescent diode (HP-SLD) was polarized and isolated by means of an isolator (I) and modulated with a polarization modulator (PM) at 128 Hz before it entered a fiber based 80/20 splitter. The reference arm consisted of a rapid scanning optical delay line (RSOD). A polarizing beam splitter (PBS) in the RSOD ensured that the reflected power was constant, regardless of the input polarization state. The sample arm contained a slit-lamp based telecentric scanner (SL), which pivoted a beam through the eye's pupil (E) by means of a set of galvanometers and two lenses. In the detector arm, light was split into two orthogonal components by means of a polarizing beam splitter and detected by two silicon detectors. At various locations in the setup, the polarization state could be tuned with polarization controllers (PC). Reprinted from reference 4 with permission from SPIE.

arm, consisting of a rapid scanning optical delay line (RSOD).[21] A polarizing beam splitter was used as a polarizer in order to ensure that light in the RSOD was always in the same linear state, regardless of changes in the polarization state in the fiber before the RSOD. A polarization controller prior to the RSOD was aligned such that the power reflected from the RSOD was constant for both input polarization states. The dispersion in sample and reference arms was matched by adjusting the grating to lens distance in the delay line. The delay line's scanning mirror was positioned off-axis and driven by a triangular waveform with a frequency of 128 Hz, synchronized with the polarization modulator, which was driven by a block wave of the same frequency. The carrier signal was at approximately 330 kHz and signals were digitally bandpass filtered with a bandwidth of 120 kHz centered at the carrier frequency. Due to the enhanced splitter ratio, seventy percent of the returned light from the sample arm went to the detection arm, while thirty percent of the light returning from the RSOD reached the detectors. The detection arm consisted of a polarization controller and a polarizing beam splitter that split the light into two orthogonal components before detection by two silicon detectors. Signal detection was shot noise limited. The two signals were digitized with a 12-bit 2.5 MHz A/D board and immediately stored to hard disk. During one B-scan, 512 A-lines over a depth of 1 mm in tissue were acquired in 2 seconds. All human experiments were performed under a protocol approved by the institutional review boards of both the Massachusetts Eye and Ear Infirmary and the Massachusetts General

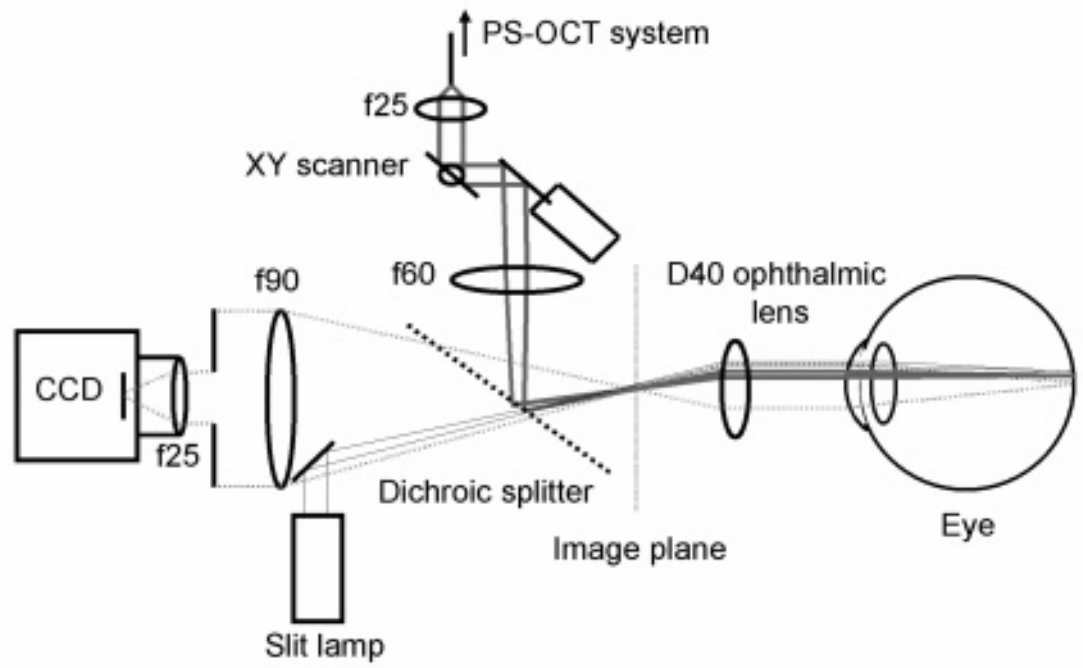

Fig. 2. Schematic overview of the optical paths in the slit-lamp. A single mode fiber guides the OCT beam into an XY galvanometer scanner. The f60 lens (f = 60 mm), positioned 60 mm from the XY galvanometer scanner in the pupil plane, focuses the PS-OCT beam in the image plane. The ophthalmic D40 lens images the PS-OCT spot of the image plane onto the retina. During scanning, the sample beam pivots in the pupil plane positioned near the corneal surface. The retina is illuminated by the incoherent source of the slit-lamp. The ophthalmic lens forms an image of the retina in the image plane, which is projected on the CCD chip through a dichroic splitter, transparent for visible light and highly reflective for near infra red light. To avoid specular reflections that decrease quality of recorded video images, the OCT beam, the illumination beam and the fixation light propagate off-axis through the D40 ophthalmic lens. Reprinted from reference 4 with permission from SPIE.

Hospital. Data from 2 volunteers were analyzed in detail. Best-corrected visual acuity was 20/20 in both volunteers. Both subjects had intraocular pressures less than 21 mmHg, normal-appearing ONHs, and normal confrontational visual fields. Volunteer 1 was 25 years old and volunteer 2 was 39 years old.

RESULTS

For the RNFL thickness analysis, structural intensity OCT images were corrected for axial motion artifacts following a method described by Swanson et al.[20] OCT intensity images were gray scale encoded on a logarithmic scale, with a white color pixel representing low reflectivity and a black pixel indicating high reflectivity. To reduce the influence of speckle noise (grainy noise caused by interference of coherent light), a moving-average filter with a length of ~7-10 μm was applied in the axial direction. The image of a circular scan was projected as a B-scan and divided into 48 sectors of 32 A-lines, each covering 7.5° of the circular scan starting temporal to the optic nerve head.

Figure 3 is a typical example of a structural intensity OCT image of the retina in the left eye of volunteer 1 obtained with a circular scan with a radius of 2.1 mm around the ONH. The image measures 13.3 mm wide × 0.9 mm deep and is shown at an expanded aspect ratio in depth for clarity. The dynamic range within the intensity image was approximately 36 dB. At the left (Fig. 3), the scan starts temporal to the ONH.

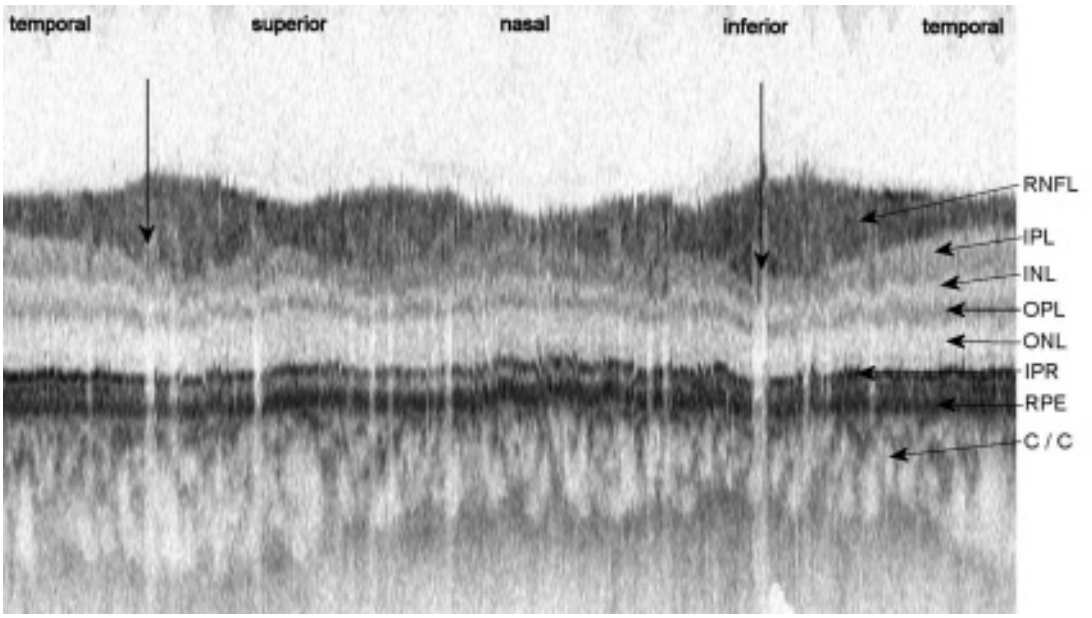

Fig. 3. Realigned OCT intensity image created with a 2.1 mm radius circular scan around the ONH. The dynamic range of the image is approximately 36 dB. Black pixels represent strong reflections. The image measures 13.3 mm wide × 0.9 mm deep. Visible structures: retinal nerve fiber layer (RNFL); inner plexiform layer (IPL); inner nuclear layer (INL); outer plexiform layer (OPL); outer nuclear layer (ONL); interface between the inner and outer segments of the photoreceptor layer (IPR); retinal pigmented epithelium (RPE); choriocapillaris and choroid (C/C). Locations of the two largest blood vessels are indicated with vertical arrows. Other smaller blood vessels that create white shadows on the RPE can be seen as well. Reprinted from reference 5 with permission from IOVS.

Structural features corresponding to different layers in the retina are evident. Based on the work done by Drexler et al; subsequent layers can be identified as follows:[11] The dark top layer is the highly scattering RNFL. At this retinal location, the thin ganglion cell layer located below the RNFL is difficult to identify. Below the RNFL we find the less scattering inner plexiform layer (IPL), the nearly transparent inner nuclear layer (INL), the scattering outer plexiform layer (OPL) and the nearly transparent outer nuclear layer (ONL). Both nuclear layers can be identified by a low reflectivity. The two dark bands below the ONL are the interface between inner and outer segments of the photoreceptor layer (IPR) and the retinal pigmented epithelium (RPE). The structure below the RPE consists of blood vessels in choriocapillaris and choroid (C). The presence of blood vessels in the RNFL at the left and right side of the image is indicated by a reduced intensity reflected from the RPE below these structures, which is attributed to signal attenuation by blood absorption. The blood vessels are marked with arrows.

For double-pass phase retardation (DPPR) calculations, two adjacent A-lines, created with two different input polarization states are necessary to calculate one DPPR A-line. In the phase retardation calculation, a considerable reduction of speckle noise was achieved by averaging the Stokes parameters of 32 adjacent A-lines with the same input polarization state. The surface Stokes vector was calculated 10 μm below the surface edge, which was determined from the I Stokes parameter in an A-line by a threshold function, preceded by a 3 × 3 median filter. Stokes vectors at the RNFL's surface were compared with Stokes vectors at lower depths to determine DPPR and optic axis orientation.[8,16,18]

In figure 4, two examples of a combined thickness and birefringence measurement are given, one of a sector superior to the optic nerve head, the other of a sector temporal to the optic nerve head. In these plots, the intensity and double pass phase retardation averaged over a sector are plotted as a function of depth. A least squares fit through data points considered to belong to the

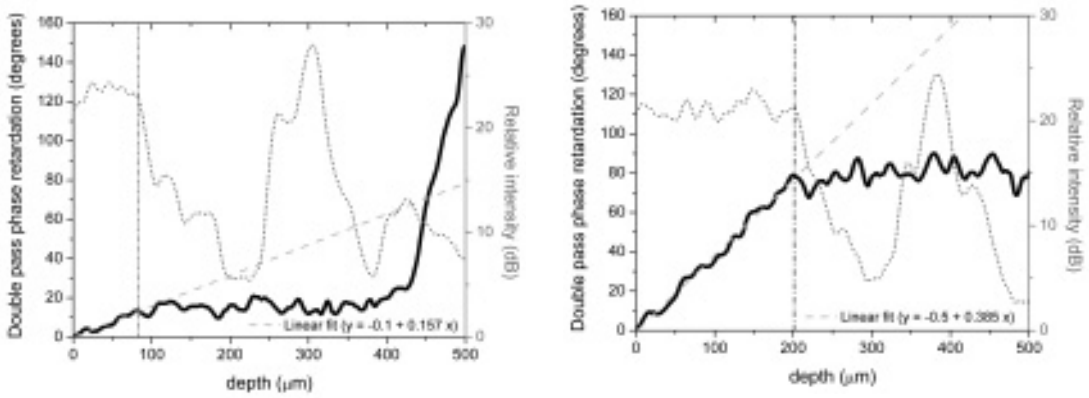

Fig. 4. Thickness and birefringence plots of an area temporal (left) and superior (right) to the optic nerve head. DPPR data belonging to the RNFL is fit with at least squares linear fit. The slope in the equation represents the DPPR/UD or birefringence. The vertical line indicates the boundary of the RNFL, as determined from the intensity and DPPR data. In the left plot, the increase in DPPR at a depth beyond 450 μm is caused by either a relatively low signal to noise ratio, or by the presence of a highly birefringent material as for instance collagen in the sclera. Reprinted from reference 5 with permission from IOVS.

RNFL is used to calculate the birefringence, or double pass phase retardation per unit depth (DPPR/UD) of the RNFL. The RNFL thickness can be determined in two ways. First, a drop in intensity is a sign of the lesser scattering ganglion cell layer and inner plexiform layer tissue below the highly scattering RNFL tissue. Second, a transition from linearly increasing double pass phase retardation to a constant value indicates a change from birefringent tissue to tissue without birefringence. The combination of these two methods helps in accurately determining the RNFL boundary. Figure 4 also demonstrates that the RNFL is birefringent and the retinal layers below the RNFL are not birefringent. The birefringence, or DPPR/UD is solely determined from the slope of the linear fit through RNFL data points in the double pass phase retardation plot, which makes this method less dependent on an accurate thickness measurement.[3-4]

RESULTS

With our PS-OCT system, thickness and birefringence were measured quantitatively as detailed above. Figure 4 is a typical example of a combined thickness and birefringence measurement obtained from volunteer 1 for a single circular scan, with the OCT structural intensity image plotted in the background. RNFL thickness and birefringence values are displayed as a function of a sector of 32 A-lines. The thickness plot indicates that the thickest RNFL is located superiorly and inferiorly. For the birefringence plot, a similar pattern is seen. The birefringence (or DPPR/UD) is relatively high superiorly and inferiorly, while it is lower temporally and nasally.

RNFL thickness and birefringence measurements

Although 12 circular scans were made in each eye, only scans outside the optic nerve head were analyzed. In general, this means that the inner two circular scans that were over the optic nerve head were not analyzed.

Thickness

In the left plot of figure 5, RNFL thickness is plotted as a function of sector and scan radius around the ONH of the left eye of volunteer 1. The smallest scan was made with a radius on the retina of 1.5 mm, while the largest scan had a radius of 2.6 mm. The different plots demon-

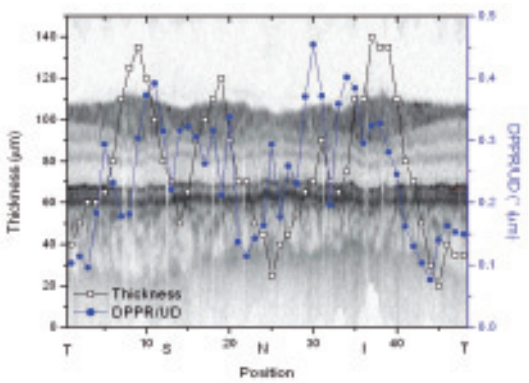

Fig. 5. A typical example of combined RNFL thickness (left axis; open squares) and birefringence (right axis; closed squares) measurements along a circular scan around the ONH. The intensity image is plotted in the background. The RNFL is relatively thicker superiorly (S) and inferiorly (I). A similar development can be seen in the birefringence plot. The birefringence is relatively higher in the thicker areas, while it is lower in the thinner temporal (T) and nasal (N) areas. Reprinted from reference 5 with permission from IOVS.

strate that an increased distance from the ONH is associated with a thinner RNFL. The thickness variation pattern with higher values inferior and superior is largely constant as a function of radius. This consistent RNFL thickness pattern can be explained by the fact that most nerves from the retina and fovea enter the ONH inferiorly and superiorly. In the right plot of figure 5, the data set of volunteer 2 shows similar characteristics as the data set of volunteer 1. One major difference is that the RNFL is thickest superior to the optic nerve head of this volunteer.

Birefringence

The same data set of volunteers 1 and 2 that were used for the thickness mapping in figure 5 were analyzed for birefringence information. All measurements per sector of 10 circular scans with increasing radius were plotted as a function of sector. In the two plots of figure 6, with the left plot containing data of volunteer 1 and volunteer 2's data in the right plot, each of 48 measurements at a certain radius is labeled with the same symbol. The mean value per sector and its standard error were plotted and neighboring means were connected with a line. The data in figure 6 was low pass filtered with an FFT based filter that retained the lowest 9 Fourier components. The processed data sets of volunteers 1 and 2 are displayed to the right of the original data sets. Thick lines represent filtered data of circular scans closer to the ONH and scans further away are marked with thinner lines.

For both subjects, the birefringence pattern is similar to the thickness pattern. At all scan radii, DPPR/UD values are relatively high in superior and inferior areas. For volunteer 1, the highest value occurs superiorly and is equal to 0.35 ± 0.03°/µm. Volunteer 2's highest value of 0.37 ± 0.04°/µm occurs inferiorly. Both volunteers exhibit low means in the temporal area: 0.10 ± 0.03°/µm (volunteer 1) and 0.11 ± 0.05°/µm (volunteer 2). For volunteer 1, the difference between the highest and lowest value is equal to 8 standard errors, indicating that the observed difference is statistically significant. The same holds for the difference observed in volunteer 2's data, which is more than 5 to 7 standard errors apart.

In areas with blood vessels, birefringence values become less reliable due to attenuation of the signal by the blood. If we were to exclude areas encompassing blood vessels, too many sectors would have been excluded. However, blood vessels become smaller and less visible in the intensity images that were taken further away from the optic nerve head. Some of them sink towards the layer below the RNFL. As a consequence, at a scan radius of 1.8 mm or more, birefringence measurements are less influenced by the presence of blood vessels.

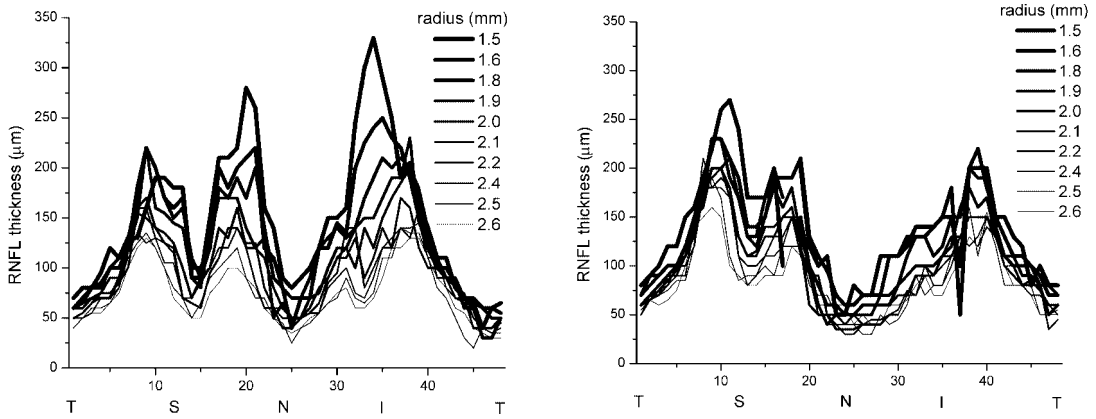

Fig. 6. RNFL thickness as a function of relative position to and distance from the ONH (left plot: left eye of volunteer 1; right plot: right eye of volunteer 2). RNFL thicknesses are given as a function of position (x axis) and scan radius (line style). Positions are relative to the ONH: temporal (T), superior (S), nasal (N) and inferior (I). Reprinted from reference 5 with permission from IOVS.

Both volunteer 1 and 2 have lower DPPR/UD values, around 0.10°/μm, temporal to the ONH. This value is equivalent to a birefringence of 1.2×10^{-4}, measured at a wavelength of 840 nm. Compared to the birefringence of a well-known birefringent material such as collagen, this value is approximately 10 times lower.[14] Superior and inferior, higher DPPR/UD values of around 0.35°/μm, equivalent to a birefringence of 4.1×10^{-4} occur.

DISCUSSION

Both thickness and birefringence of the RNFL vary as a function of sector on a circle around the optic nerve head. The thickness variation is a consequence of the thicker superior and inferior nerve bundles, compared to the temporal and nasal sectors. With increasing radius, the RNFL becomes thinner in all sectors. The birefringence variation can not be explained by the RNFL thickness variation, since birefringence is a material property independent of the sample thickness. Difference in birefringence indicates differences in structure of the sample. In the retina this could be related to nerve bundle diameter or other micro structural anatomical differences in the RNFL. In contrast to RNFL thickness, RNFL birefringence seems to be constant with increasing scan radius.

Our measurements demonstrate that in the healthy retina of two young volunteers, the RNFL birefringence or DPPR/UD varies as a function of sector around the ONH, with lowest values (0.10°/μm) occurring temporally and highest values (ca. 0.35°/μm) occurring inferiorly and superiorly. In SLP, a constant birefringence or DPPR/UD value is used as a conversion factor to convert measured DPPR to RNFL thickness. Since DPPR/UD varies as a function of sector, SLP phase retardation to thickness conversion will not yield accurate RNFL thickness values for all sectors.

Our DPPR/UD measurement does not rely on an accurate determination of the RNFL thickness. The DPPR/UD is determined from the slope of the phase retardation with depth as determined from a PS-OCT depth resolved phase retardation measurement.

Weinreb et al. found a correlation between RNFL thickness and phase retardation from different locations in the primate retina, but they did not consider different birefringence values as a function of sector, which could explain the considerable variation around the regression line.[22]

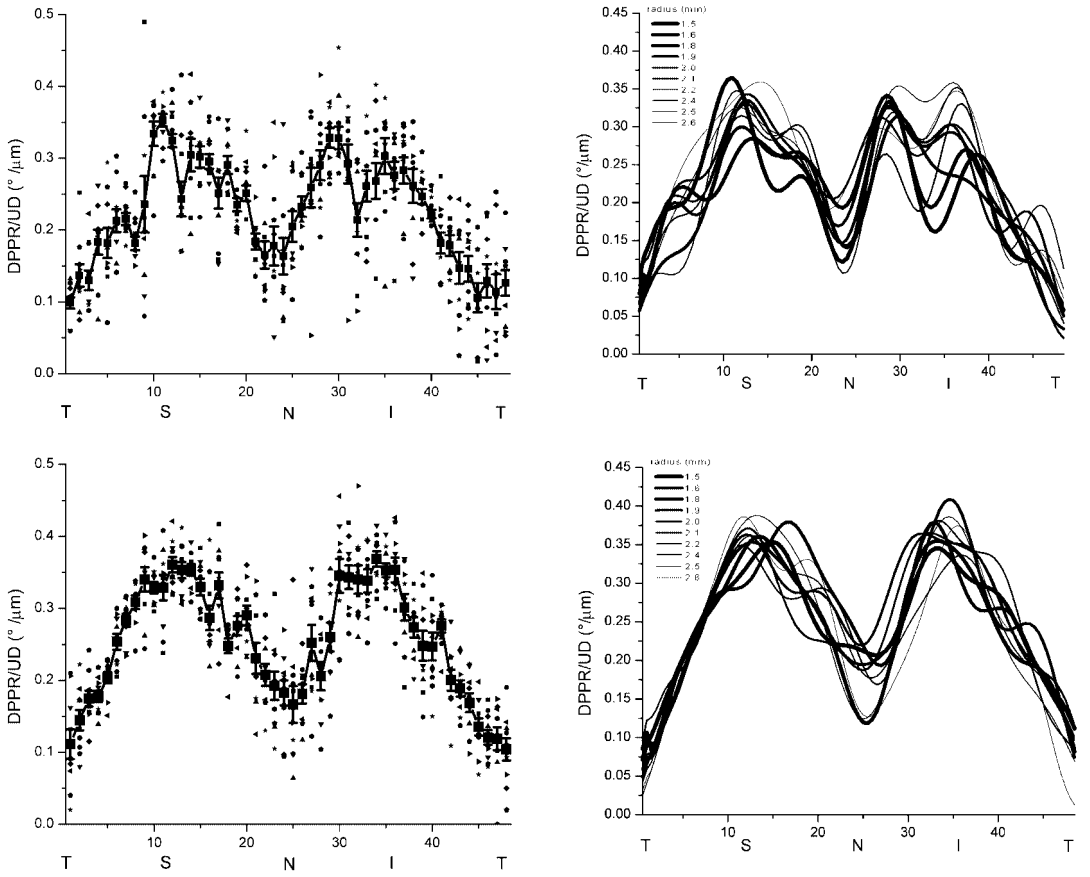

Fig. 7. At the left, the RNFL birefringence is plotted as a function of relative position with respect to the ONH (upper left plot: left eye of volunteer 1; lower left plot: right eye of volunteer 2). Birefringence was measured in all 48 sectors of 10 scans with radii between 1.5 and 2.6 mm around the ONH. Results from sectors at a certain radius are marked with the same symbol. The mean birefringence was marked with a larger symbol and connected with a line. Error bars indicate the standard error. At the right, the same data after filtering with a low pass FFT filter ($f_{cut\text{-}off}$ = 0.125 Hz) reveals possible trends in DPPR/UD as a function of radius and tells whether averaging is permitted. Reprinted from reference 5 with permission from IOVS.

CONCLUSION

Birefringence of healthy RNFL is constant as a function of scan radius but varies as a function of position around the ONH, with higher values occurring superior and inferior to the ONH. Measured DPPR/UD values around the ONH of two healthy subjects varied between 0.10 and 0.35°/μm. These values are equivalent to birefringence values of 1.2×10^{-4} and 4.1×10^{-4}, measured at a wavelength of 840 nm. Consequently, when assuming a spatially constant birefringence value around the optic nerve head, the conversion of SLP phase retardation measurements may yield incorrect thickness values. Difference in birefringence between superior/inferior and temporal/nasal regions indicate micro structural differences in the nerve fiber layer anatomy, possibly related to nerve bundle diameter or density.

ACKNOWLEDGEMENTS

The authors acknowledge research grants from the National Eye Institute (1R 24 EY 12877) and Whitaker Foundation (26083) and a gift from Dr. and Mrs. J. S. Chen to the Optical Diagnostics Program of the Wellman Center for Photomedicine for the support of this research.

REFERENCES

(1) AMERICAN NATIONAL STANDARDS INSTITUTE – American National Standard for Safe Use of Lasers Z136.1. Laser institute of America, Orlando FL 2000
(2) CAMPBELL F.W., GREEN D.G. – Optical and Retinal Factors Affecting Visual Resolution. J Physiol London 1965; 181: 576
(3) CENSE B., CHEN T.C., PARK B.H., PIERCE M.C., DE BOER J.F. – In vivo depth-resolved birefringence measurements of the human retinal nerve fiber layer by polarization-sensitive optical coherence tomography. Opt Lett 2002; 27: 1610-1612
(4) CENSE B., CHEN T.C., PARK B.H., PIERCE M.C., DE BOER J.F. – In vivo birefringence and thickness measurements of the human retinal nerve fiber layer using polarization-sensitive optical coherence tomography. J Biomed Optics 2004; 9: 121-125
(5) CENSE B., CHEN T.C., PARK B.H., PIERCE M.C., DE BOER J.F. – Thickness and birefringence of healthy retinal nerve fiber layer tissue measured with polarization sensitive optical coherence tomography. Invest Ophthalmol Vis Sci 2004; 45: 2606-2612
(6) CENSE B., NASSIF N., CHEN T.C., PIERCE M.C., YUN S.H., PARK B.H., BOUMA B.E., TEARNEY G.J., DE BOER J.F. – Ultrahigh-Resolution High-Speed Retinal Imaging Using Spectral-Domain Optical Coherence Tomography. Optics Express 2004; 12: 2435-2447
(7) DE BOER J.F., MILNER T.E., VAN GEMERT M.J.C., NELSON J.S. – Two-dimensional birefringence imaging in biological tissue by polarization-sensitive optical coherence tomography. Optics Letters 1997; 22: 934-936
(8) DE BOER J.F., MILNER T.E., NELSON J.S. – Determination of the depth-resolved Stokes parameters of light backscattered from turbid media by use of polarization-sensitive optical coherence tomography. Optics Letters 1999; 24: 300-302
(9) DUCROS M.G., DE BOER J.F., HUANG H.E., CHAO L.C., CHEN Z.P., NELSON J.S., MILNER T.E., RYLANDER H.G. – Polarization sensitive optical coherence tomography of the rabbit eye. IEEE Journal of Selected Topics in Quantum Electronics 1999; 5: 1159-1167
(10) DUCROS M.G., MARSACK J.D., RYLANDER H.G., THOMSEN S.L., MILNER T.E. – Primate retina imaging with polarization-sensitive optical coherence tomography. Journal of the Optical Society of America A 2001; 18: 2945-2956
(11) DREXLER W., SATTMANN H., HERMANN B., KO T.H., STUR M., UNTERHUBER A., SCHOLDA C., FINDL O., WIRTITSCH M., FUJIMOTO J.G., FERCHER A.F. – Enhanced visualization of macular pathology with the use of ultrahigh-resolution optical coherence tomography. Arch Ophthalmol 2003; 121: 695-706
(12) GREENFIELD D.S., KNIGHTON R.W., HUANG X.R. – Effect of corneal polarization axis on assessment of retinal nerve fiber layer thickness by scanning laser polarimetry. Am J Ophthalmol 2000; 129: 715-722
(13) HUANG X.R., KNIGHTON R.W. – Linear birefringence of the retinal nerve fiber layer measured in vitro with a multispectral imaging micropolarimeter. J Biomed Optics 2002; 7: 199-204
(14) MAITLAND D.J., WALSH J.T. – Quantitative measurements of linear birefringence during heating of native collagen. Lasers in Surgery & Medicine 1997; 20: 310-318
(15) NASSIF N., CENSE B., PARK B.H., PIERCE M.C., YUN S.H., BOUMA B.E., TEARNEY G.J., CHEN T.C., DE BOER J.F. – In vivo high-resolution video-rate spectral-domain optical coherence tomography of the human retina and optic nerve. Optics Express 2004; 12: 367-376
(16) PARK B.H., SAXER C., SRINIVAS S.M., NELSON J.S., DE BOER J.F. – In vivo burn depth determination by high-speed fiber-based polarization sensitive optical coherence tomography. J Biomed Optics 2001; 6: 474-479
(17) QUIGLEY H.A., ADDICKS E.M., GREEN W.R. – Optic nerve damage in human glaucoma. III. Quantitative correlation of nerve fiber loss and visual field defect in glaucoma, ischemic neuropathy, papilledema, and toxic neuropathy. Arch Ophthalmol 1982; 100: 135-146

(18) SAXER C.E., DE BOER J.F., PARK B.H., ZHAO Y.H., CHEN Z.P., NELSON J.S. – High-speed fiber-based polarization-sensitive optical coherence tomography of in vivo human skin. Optics Letters 2000; 25: 1355-1357
(19) SCHUMAN J.S., HEE M.R., PULIAFITO C.A., WONG C., PEDUT-KLOIZMAN T., LIN C.P., HERTZMARK E., IZATT J.A., SWANSON E.A., FUJIMOTO J.G. – Quantification of nerve fiber layer thickness in normal and glaucomatous eyes using optical coherence tomography. Arch Ophthalmol 1995; 113: 586-596
(20) SWANSON E.A., IZATT J.A., HEE M.R., HUANG D., LIN C.P., SCHUMAN J.S., PULIAFITO C.A., FUJIMOTO J.G. – In-Vivo Retinal Imaging by Optical Coherence Tomography. Optics Letters 1993; 18: 1864-1866
(21) TEARNEY G.J., BOUMA B.E., FUJIMOTO J.G. – High-speed phase- and group-delay scanning with a grating-based phase control delay line. Optics Letters 1997; 22: 1811-1813
(22) WEINREB R.N., DREHER A.W., COLEMAN A., QUIGLEY H., SHAW B., REITER K. – Histopathalogic Validation of Fourier-Ellipsometry Measurements of Retinal Nerve Fiber Layer Thickness. Arch Ophthalmol 1990; 108: 557-560
(23) WEINREB R.N., BOWD C., ZANGWILL L.M. – Glaucoma detection using scanning laser polarimetry with variable corneal polarization compensation. Arch Ophthalmol 2003; 121: 218-224
(24) ZHOU Q., KNIGHTON R.W. – Light Scattering and Form Birefringence of Parallel Cylindrical Arrays that Represent Cellular Organelles of the Retinal Nerve Fiber Layer. Appl Opt 1997; 36: 2273-2285
(25) ZHOU Q.Y., WEINREB R.N. – Individualized compensation of anterior segment birefringence during scanning laser polarimetry. Invest Ophthalmol Vis Sci 2002; 43: 2221-2228

.....

Corresponding Address:

Johannes F. de Boer, PhD
Wellman Center for Photomedicine, Massachusetts General Hospital
50 Blossom Street, BAR 724
Boston, MA 02114
Email: deboer@helix.mgh.harvard.edu